Supplemental Figures

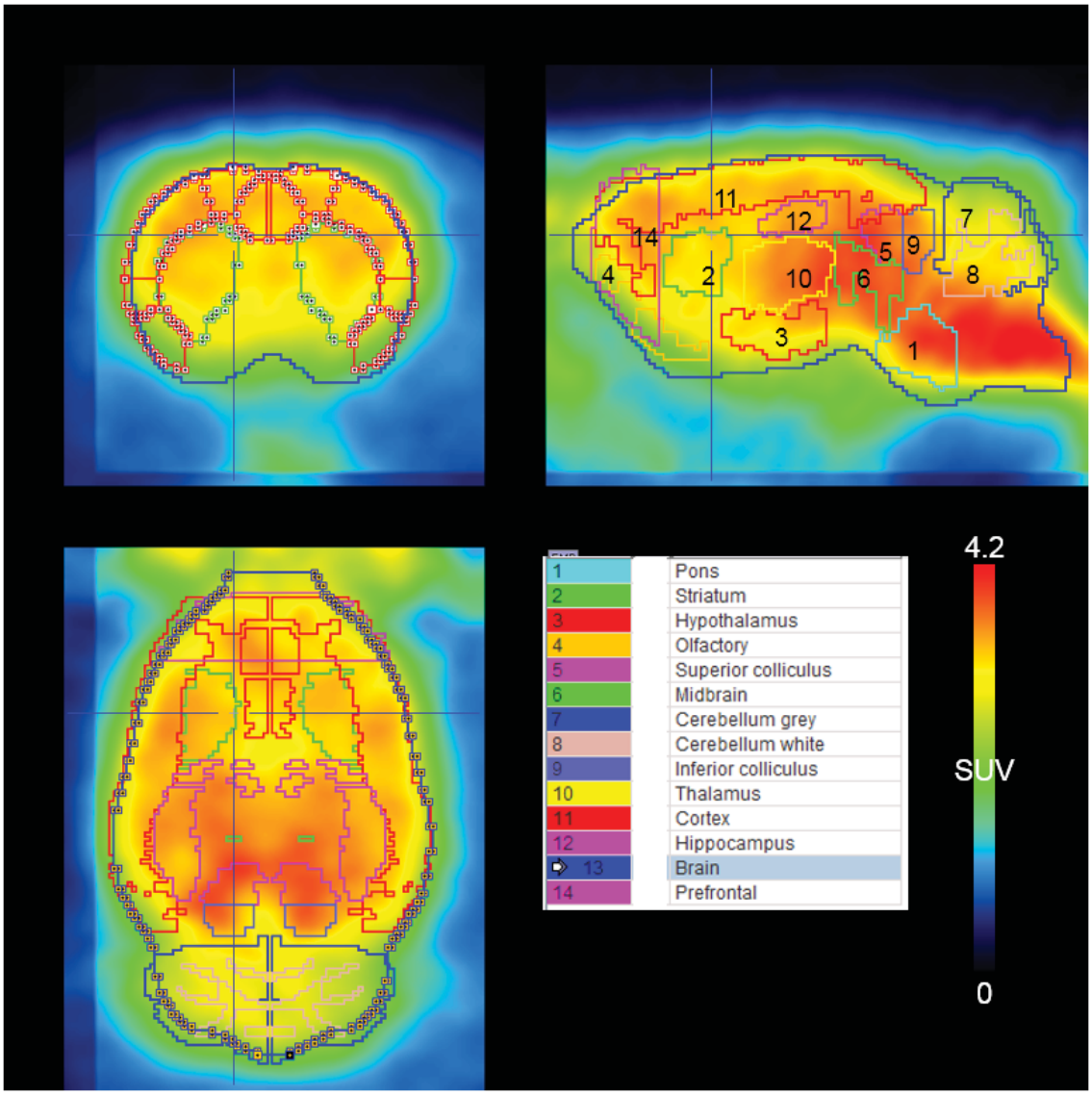

Supplemental Figure 1. ^{11}C-Me-NB1 PET images of rat brain, averaged from 3 individual scans, 0 to 60 min after tracer injection. PET data were reconstructed with 2D Fourier rebinning/ordered-subsets expectation maximization algorithms (FORE/OSEM), 2 iterations, 16 subsets, into time frames between 20 and 180 s for kinetic modelling with an input function or between 120 and 300 s for scans without an input function. PET data were corrected for singles and randoms but not for attenuation. The brain region template used for the quantitative analysis is superimposed (PMOD). The volumes (mm^3) of the individual regions of interest were pons, 45; striatum, 87; hypothalamus, 37; olfactory, 28; superior colliculus, 14; midbrain, 23; cerebellum grey matter, 150; cerebellum white matter, 47; inferior colliculus, 11; thalamus, 61; cortex, 576; hippocampus, 70; whole brain, 1831; prefrontal cortex, 132. The standardized uptake values (SUV) were calculated as Bq per g tissue divided by injected Bq per g body weight. The SUV corresponds to % injected dose per g tissue multiplied with body weight (g) and divided by 100 %. Specific binding in % in the *ex vivo* biodistribution experiments were calculated as (SUV(baseline)-SUV(blockade))/SUV(baseline)*100.

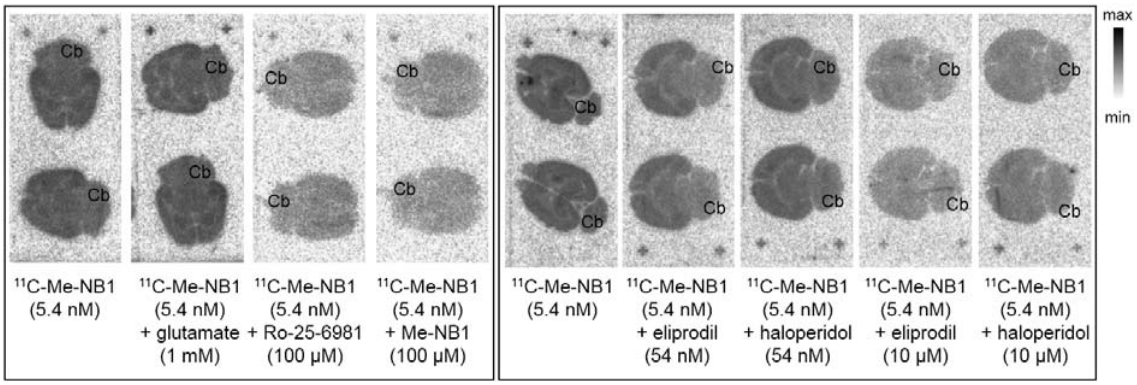

Supplemental Figure 2. Characterization of ^{11}C-Me-NB1 binding to rat brain tissue by *in vitro* autoradiography. Baseline and blocking conditions as indicated. Results from two independent experiments as indicated by the frames. Cb, cerebellum, for orientation. Intensity bar with maximal (max) and minimal (min) unmodified phosphorimager signal intensity (a.u.). Horizontal rat brain slices (20 µm) of adult male Wistar rats were incubated for 30 min at room temperature with ^{11}C-Me-NB1 alone or in combination with the indicated compounds, in HEPES buffer (30 mM HEPES, 110 mM NaCl, 5 mM KCl, 2.5 mM $CaCl_2$, 1.2 mM $MgCl_2$, pH 7.4) containing 0.1 % bovine serum albumin (HEPES/BSA). After incubation, the slices were washed with HEPES/BSA (8 min), HEPES buffer (2×3 min) and water (2×5 s). The dried slices were exposed for 20 min to a phosphorimager plate and read in a phosphorimager BAS5000 (Fuji, Tokyo, Japan; software AIDA v4.5). Radioactivity accumulation was quantified with the software PMOD v3.7 (PMOD Technologies, Zurich, Switzerland). Note that the bivalent cations in the HEPES buffer could affect ^{11}C-Me-NB1 binding (*1*).

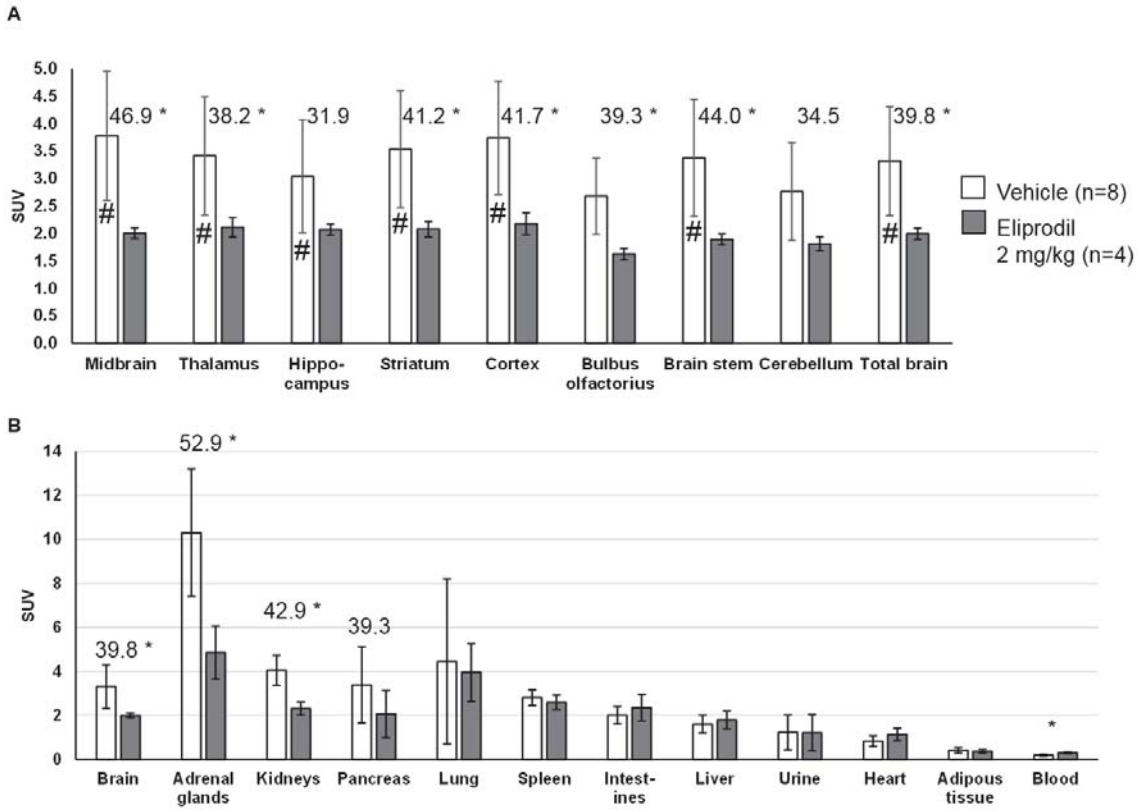

Supplemental Figure 3. Distribution of ^{11}C-Me-NB1 in rat tissues determined by dissection 15 min after ^{11}C-Me-NB1 i.v. injection under baseline and blocking conditions, as indicated. Numbers show the percent specific binding. * indicates significant reduction (increase in the case of blood) by eliprodil ($p < 0.05$). # indicates significantly higher SUV than cerebellum under baseline conditions ($p < 0.01$, paired t-test, not corrected for multiple comparisons). **A**) Brain regions. **B**) All tissues, including whole brain (calculated from the SUV and tissue weights in **A**).

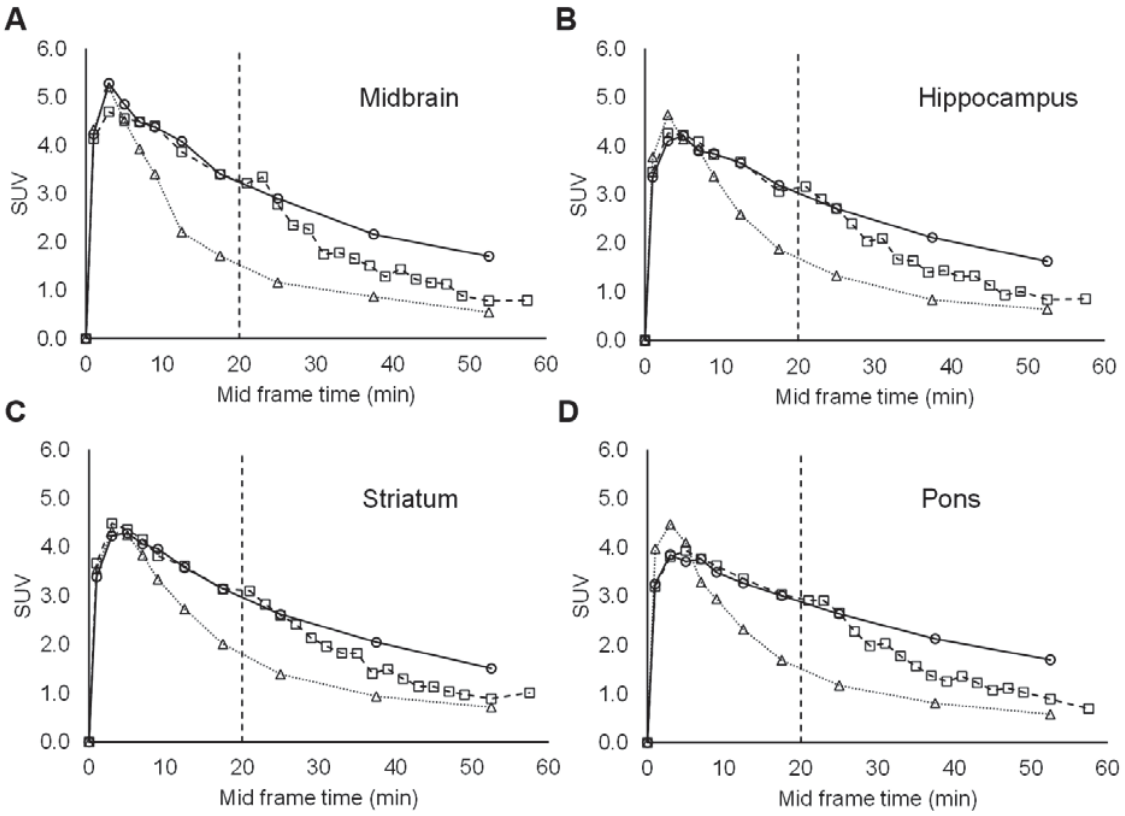

Supplemental Figure 4. Brain region TACs of ^{11}C-Me-NB1 under baseline, blocking and displacement conditions. Same scans and conditions as shown in **Fig. 2**. ○, Baseline; △, blockade with 1 mg/kg eliprodil (1 min before tracer injection); □, displacement with 1 mg/kg eliprodil (20 min after tracer injection, indicated by vertical broken lines). **A**) Midbrain, **B**) hippocampus, **C**) striatum, **D**) pons.

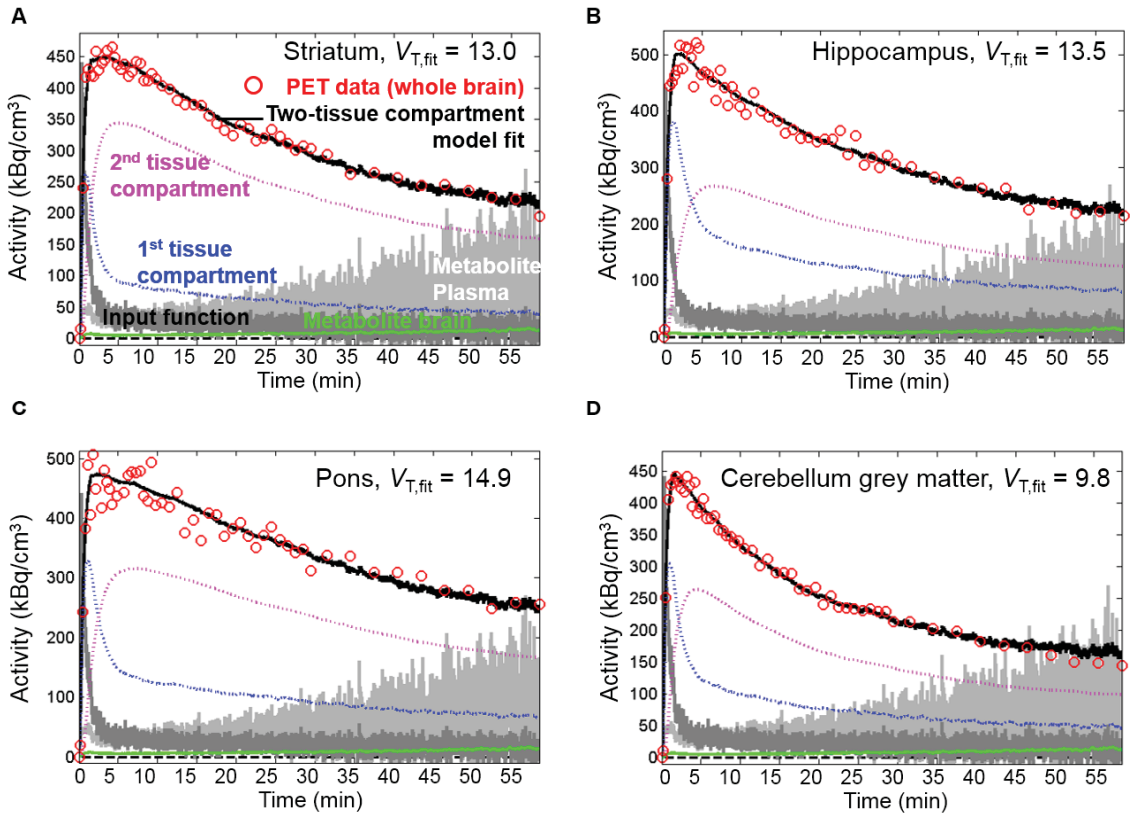

Supplemental Figure 5. ^{11}C-Me-NB1 TACs and kinetic modeling for individual brain regions of the scan shown in **Fig. 3**. **A**) Striatum, **B**) hippocampus, **C**) pons, **D**) cerebellum grey matter. ○, experimental data; lines, dark grey, input function; light grey, input function of radiometabolite; black solid, fit TAC; pink dotted, tracer simulated in 2nd tissue compartment (specific binding); blue dotted, tracer simulated in 1st tissue compartment (non-displaceable); green, radiometabolite simulated in brain. The respective $V_{T,fit}$ (mL/cm^3) are shown in the panels. Ratio parent/total radioactivity in plasma and brain: in a pilot experiment, a rat (339 g) was injected into a lateral tail vein 81.8 MBq ^{11}C-Me-NB1 under isoflurane anesthesia and sacrificed 5 min later by decapitation under anesthesia. The blood was collected and plasma was separated by centrifugation (5000 × g, 5 min, 4°C). The brain was homogenized in an equivalent volume of ice cold PBS for 1-2 min. The proteins in both samples were precipitated with equivalent volumes of ice cold acetonitrile and centrifugation as above. The analysis of the filtered supernatants by TLC (silica gel, MERCK KGaA; mobile phase, methanol) and the phosphorimager revealed a single, polar radiometabolite beside the parent tracer. To determine the ratio of parent tracer to total radioactivity in plasma and brain over time, 6 rats (227-421 g) were injected into a lateral tail vein with 28-37 MBq ^{11}C-Me-NB1 and blood samples were drawn from the opposite vein at the indicated time points. The rats were sacrificed at 15, 30 and 60 min, respectively, and brains and blood were collected. Blood and brain samples were processed as above. The unfiltered supernatants after acetonitrile addition were diluted with 3 volumes of water. The solution was passed through a Sep-Pak C18 Light cartridge (Waters, Milford, MA) and washed with 1 mL water. The combined aqueous phase contained the polar radiometabolite. The parent compound was eluted with 1 mL ethanol. The separation was confirmed by TLC. The radioactivity in both aqueous and ethanol eluents was quantified in the gamma counter and the ratio parent to total radioactivity was calculated as the radioactivity in the ethanol phase divided by the sum of the radioactivity in both

phases. The ratio of plasma to whole blood radioactivity was determined from plasma and whole blood in the gamma counter, it was 1.11. Kinetic modeling: Scans with an input function were analyzed based on a two-tissue compartment model (*2*) with a home-written MATLAB script (MathWorks, Natick, MA). PET TACs and not-decay corrected blood coincidences were loaded. The start time of the blood coincidences curve and the background coincidences were estimated as the time point of the first significant increase in the data and the average counts before this time point, respectively. Both values were refined during the fitting procedure. The background- and start time-corrected coincidences were decay-corrected and multiplied with the experimentally determined calibration factor between the PET scanner and the coincidence counter and the plasma/blood radioactivity ratio of 1.11. They were further multiplied with a bi-exponential function (refined during the fitting procedure) to correct for the experimentally determined ratio parent/total radioactivity in plasma and the radiometabolite input function was revealed as the difference between the total and parent coincidences. These adapted input functions were convoluted with the weighting function for a two-tissue compartment model for the parent tracer, defined by K_1, k_2, k_3 and k_4, and a one-tissue compartment model for the radiometabolite, defined by K_{1M} and k_{2M} (*2*). The squared residuals between the experimental data and the fit functions for the brain TAC (consisting of parent tracer, radiometabolite and blood radioactivity, assuming a partial volume of 5 % blood in the brain), as well as fit functions for the parent/total radioactivity in plasma and brain were minimized with the function fmincon and a multistart procedure with 64 runs. For whole brain, the difference between $V_{T,fit}$ and $V_{T,Logan}$, determined from the Logan plot (*3*), were furthermore minimized to allow to accurately define the starting time and background coincidences of the blood coincidence curve. In addition, the 4 parameters defining the ratio parent/total radioactivity in plasma were fit. In summary, the following parameters were fit simultaneously: K_1, k_2, k_3, k_4, input function start time, blood coincidence background, A, B, a and b of the function parent/total radioactivity in plasma = $A\times\exp(-a\times t)+B\times\exp(-b\times t)+(1-A-B)$, furthermore K_{1M} and k_{2M}. The parameters were fit by minimizing the differences between the fit and experimental brain TAC, the fit and experimental plasma and brain ratios parent tracer/total radioactivity and the $V_{T,fit}$ and $V_{T,Logan}$. The resulting start time and background coincidences of the blood coincidence curve and the bi-exponential function defining the parent/total radioactivity ratio in plasma were then fixed to analyze the stability of K_1 to k_4 and the composite parameters for whole brain at truncated scan durations and for the individual brain regions at full scan time, in 8 runs each (multistart with fmincon). For comparison, K_{1M} was fixed at 0, ignoring radiometabolite distribution to the brain.

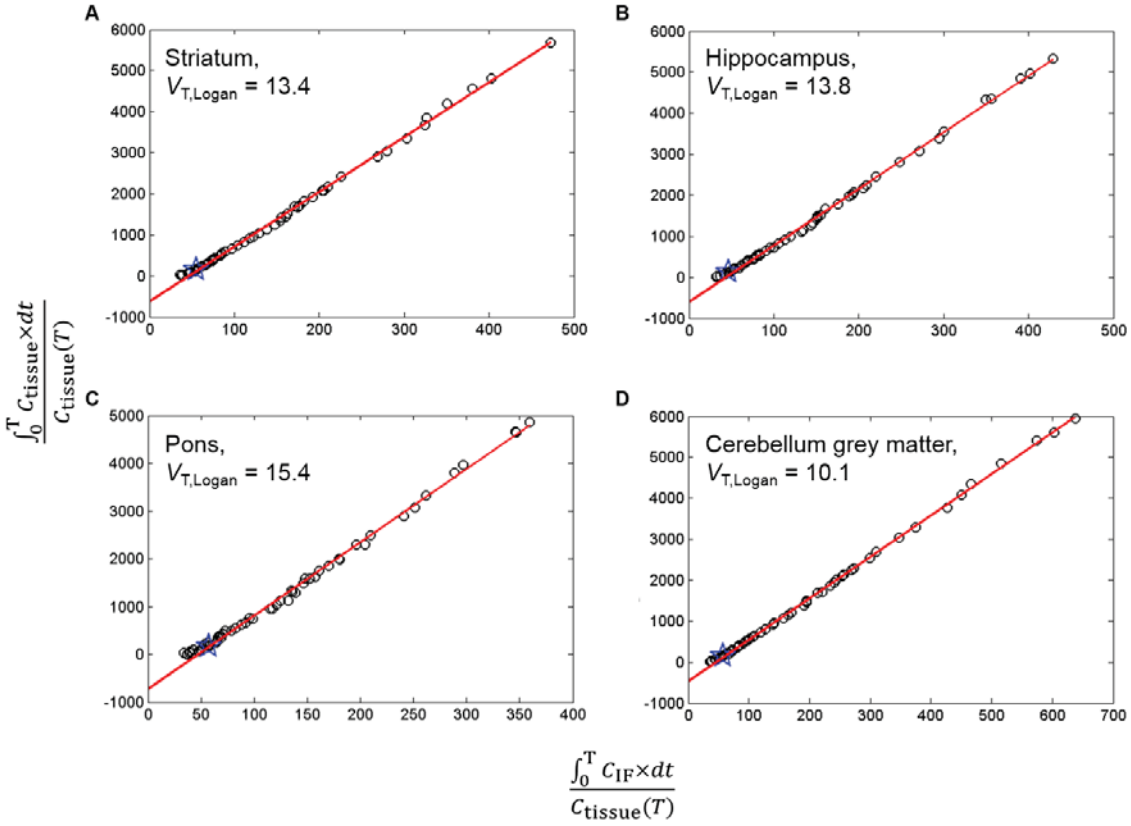

Supplemental Figure 6. Logan plots for individual brain regions of the scan shown in **Figure 3** and **Supplemental Figure 5**. **A**) Striatum, **B**) hippocampus, **C**) pons, **D**) cerebellum grey matter. Symbols and lines as indicated in **Figure 3** in the manuscript. The respective $V_{T,Logan}$ (mL/cm^3) are shown in the panels.

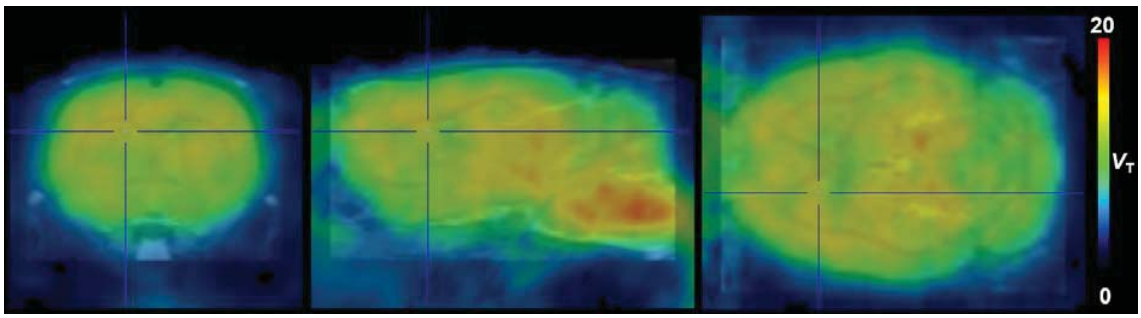

Supplemental Figure 7. Parametric maps for V_T (mL/cm^3) for the scan shown in **Fig. 2A**. The maps were generated with PMOD v3.8 based on the input function (see above) and the image data. Vertical (left), sagittal (middle), horizontal (right) planes at 1.7 mm (left-right), 3.8 mm (dorsal-ventral), 0.4 mm (anterior-posterior) from Bregma (as in **Fig. 2A**).

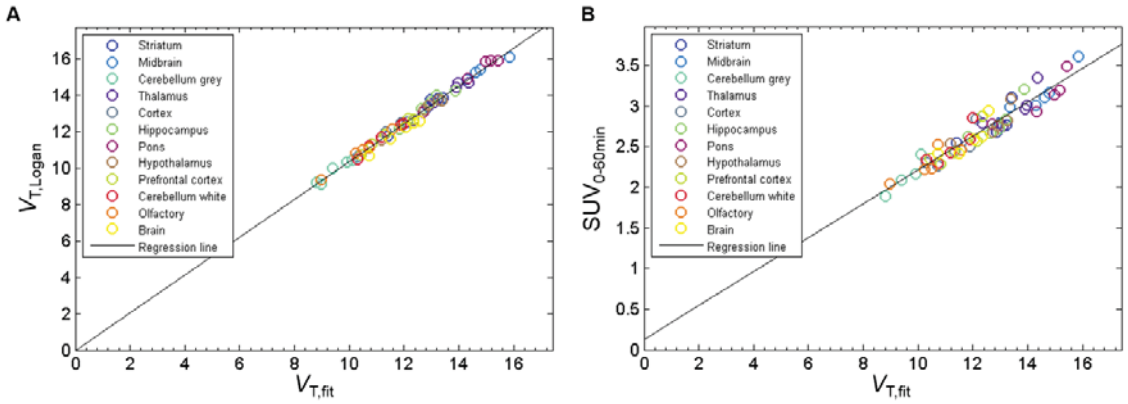

Supplemental Figure 8. Comparison of $V_{T,Logan}$ and $SUV_{0-60min}$ with $V_{T,fit}$. **A**) $V_{T,Logan}$ *vs* $V_{T,fit}$ of 5 scans and 12 brain regions each. The correlation was $V_{T,Logan} = 1.04 \times V_{T,fit} - 0.03$ mL/cm^3 ($r^2 = 0.99$). **B**) $SUV_{0-60min}$ *vs* $V_{T,fit}$ (same scans and regions as in **A**). The correlation was $SUV_{0-60min} = (0.209$ cm^3/mL$) \times V_{T,fit} + 0.123$; $r^2 = 0.913$.

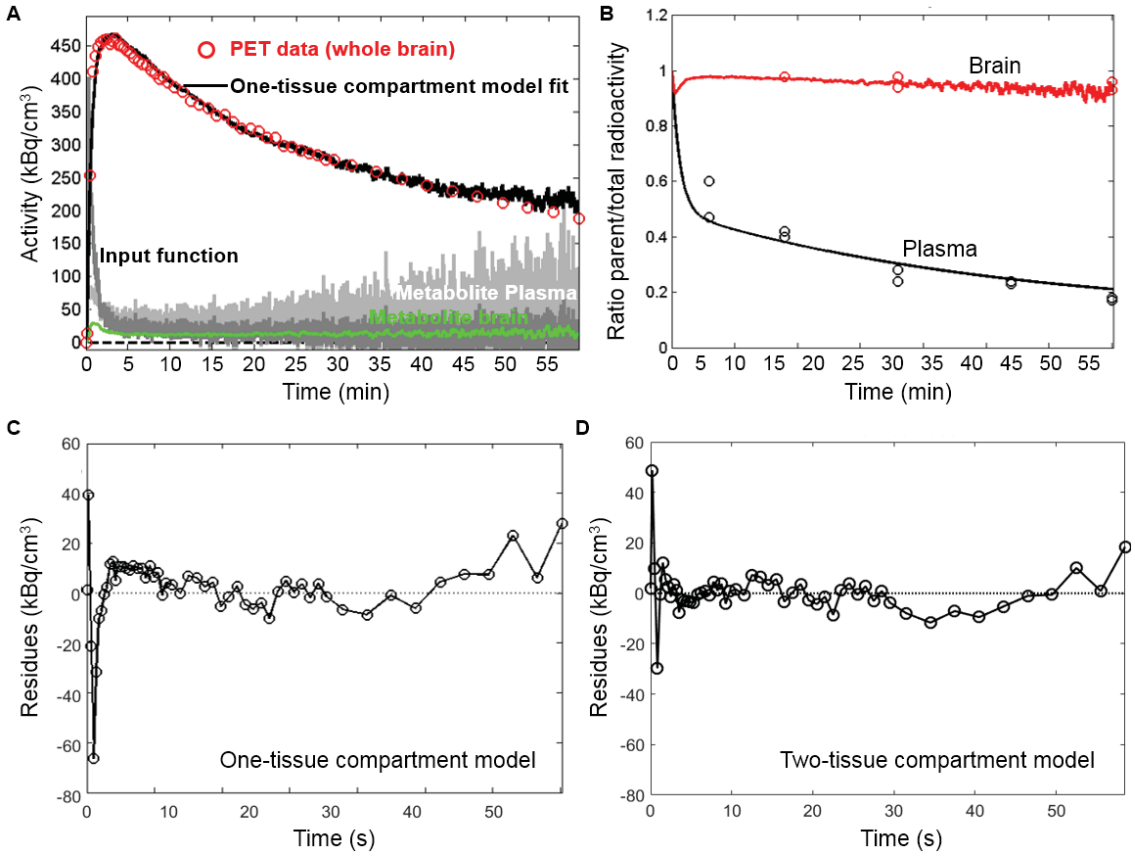

Supplemental Figure 9. The experimental brain TAC shown in **Fig. 3** fit to one-tissue compartment models for both the parent tracer and the radiometabolite. **A**) Fit brain TAC. **B**) Simultaneously fit ratios parent tracer to total radioactivity in brain and plasma. **C**) Residuals for the brain TAC fit with a one-tissue compartment model each for parent tracer and radiometabolite. The corrected Akaike information criterion was 317.9. **D**) Residuals for the brain TAC fit with a two-tissue compartment model for the parent tracer and a one-tissue compartment model for the radiometabolite (residuals from fit shown in **Fig. 3A**), The Akaike information criterion was 266.1. Deviations from the experimental parent/total radioactivity ratios in plasma and brain were not included in the calculations of the Akaike information criterion. The model with the lower Akaike information criterion is the preferred model.

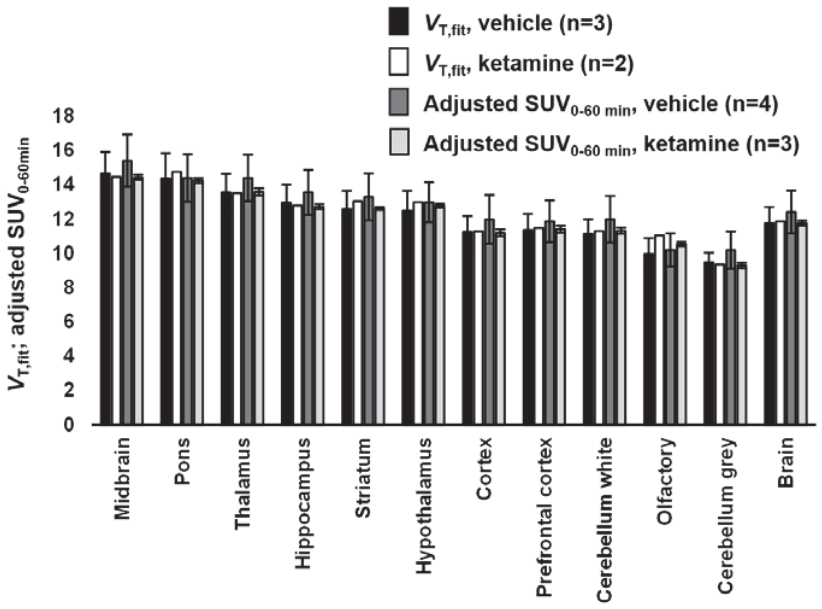

Supplemental Figure 10. Quantitative PET with and without an input function and influence of ketamine on ^{11}C-Me-NB1 PET. $V_{T,fit}$ values (mL/cm^3) from kinetic modeling and adjusted $SUV_{0-60min}$ as ($SUV_{0-60min}$-0.123)/(0.209 cm^3/mL), according to **Supplemental Figure 8B**. Scans without a meaningful input function were included for the adjusted $SUV_{0-60min}$. Mean values with standard deviations (for $n \geq 3$), n as indicated. To study the influence of ketamine and glutamate *in vivo*, 3 of the 7 rats with input-function recording were administered intraperitoneally 25 mg/kg ketamine 30 min before tracer injection. The $V_{T,fit}$ values of the 2 ketamine-treated rats with complete input function were within the standard deviations of the respective values from the baseline scans or close to this range (**Supplemental Tables 3 and 4**) and no significant difference was detected between the respective $SUV_{0-60min}$ values. This excludes a major influence of the ketamine challenge on ^{11}C-Me-NB1 accumulation in rat brain under isoflurane anesthesia. $V_{T,fit}$ and adjusted SUV of all brain regions except olfactory bulb were significantly higher than the respective parameter of cerebellum grey matter ($p < 0.05$, paired t-test, not corrected for multiple comparisons and not analyzed for $n < 3$).

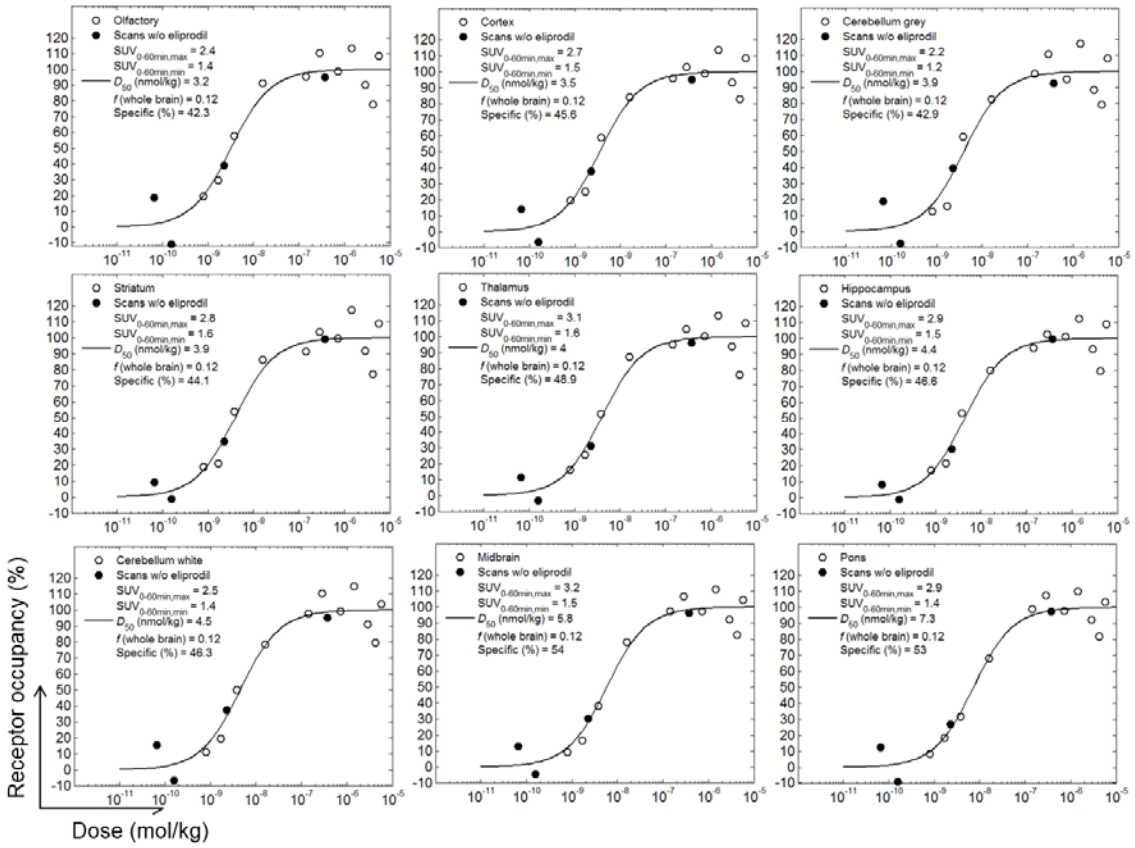

Supplemental Figure 11. Receptor occupancy by eliprodil as determined by PET with ^{11}C-Me-NB1 in individual brain regions as indicated. The regions and fit parameters are indicated in the panels.

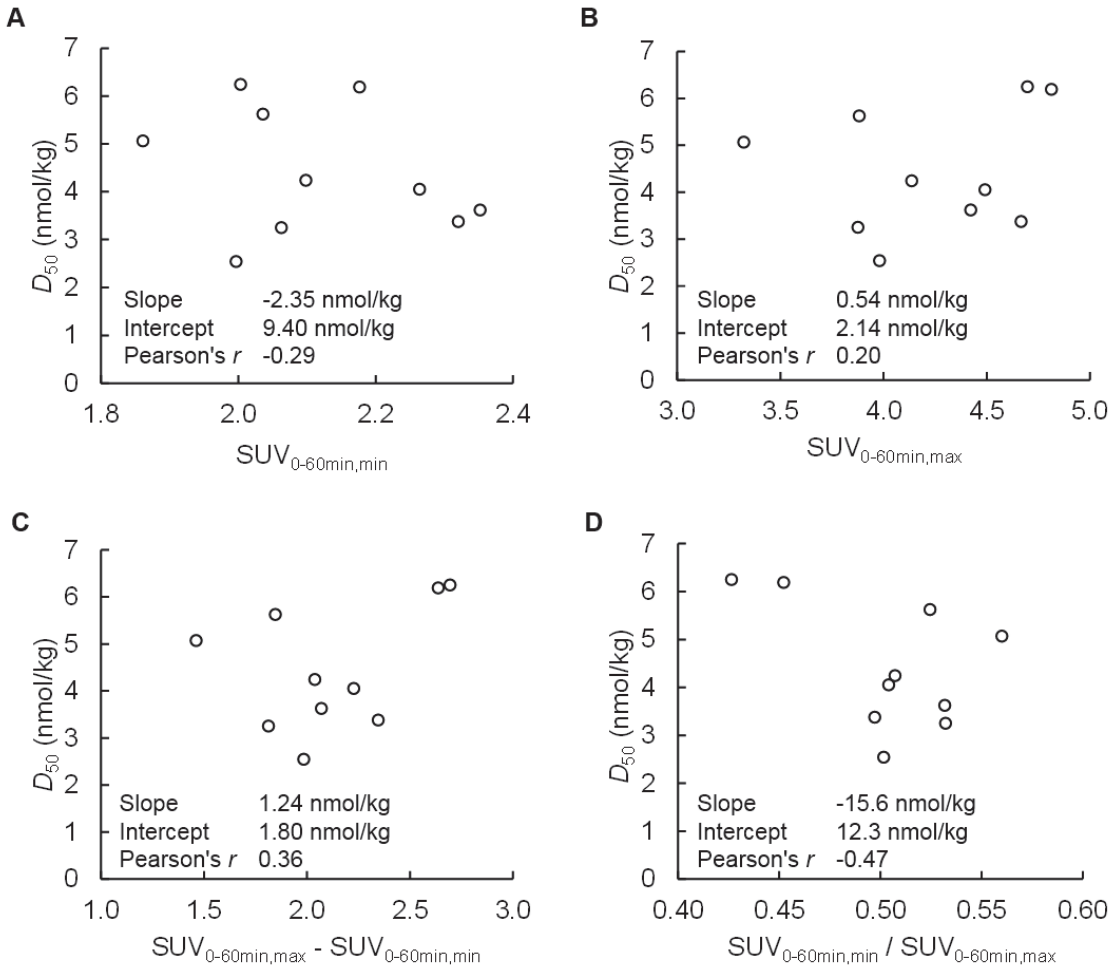

Supplemental Figure 12. Weak or absent correlation between D_{50} and fitted non-displaceable tracer accumulation ($SUV_{0\text{-}60min,min}$). $SUV_{0\text{-}60min,max}$ and $SUV_{0\text{-}60min,min}$ are the fitted maximal and minimal $SUV_{0\text{-}60min}$ of the receptor occupancy data of the various brain regions (**Fig. 4** and **Supplemental Fig. 11**). **A**) D_{50} *vs* $SUV_{0\text{-}60min,min}$. **B**) D_{50} *vs* $SUV_{0\text{-}60min,max}$. **C**) D_{50} *vs* $SUV_{0\text{-}60min}$ of specifically bound tracer. **D**) D_{50} *vs* the relative $SUV_{0\text{-}60min,min}$. Linear regression analysis results are shown in the panels.

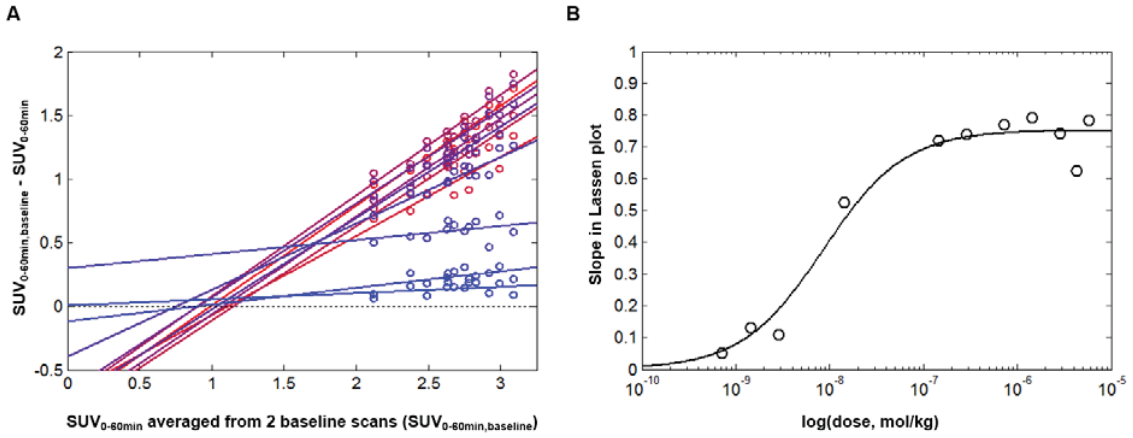

Supplemental Figure 13. Receptor occupancy estimated from the Lassen plot. **A**) Lassen plot according to Cunningham et al. (*4*). $SUV_{0\text{-}60min,baseline}$ was averaged from the two baseline scans with the lowest ^{11}C-Me-NB1 dose in nmol/kg, i.e., 0.5 and 1.3 nmol/kg (x-axis). The differences between the averaged regional baseline $SUV_{0\text{-}60min}$ values and the regional $SUV_{0\text{-}60min}$ values after eliprodil administration are plotted on the y-axis (increasing eliprodil dose from blue to red color). Under ideal conditions, the slope of the Lassen plot (symbols, linear regression of the data points at a particular dose, lines) equals the receptor occupancy as a fraction of 1 and the intercept with the x-axis equals the $SUV_{0\text{-}60min}$ in the absence of specific binding (*4*). **B**) ○, Slopes of the Lassen plot in **A**. Solid line, fit with a saturation function, the minimum was fixed at 0 and receptor occupancy by the tracer was neglected. Fitted D_{50} (eliprodil dose at 50 % of fitted maximal occupancy) was 8.5 nmol/kg. Note that the Lassen plot assumes equal D_{50} and $SUV_{0\text{-}60min,min}$ for all brain regions and neglects occupancy by the tracer itself.

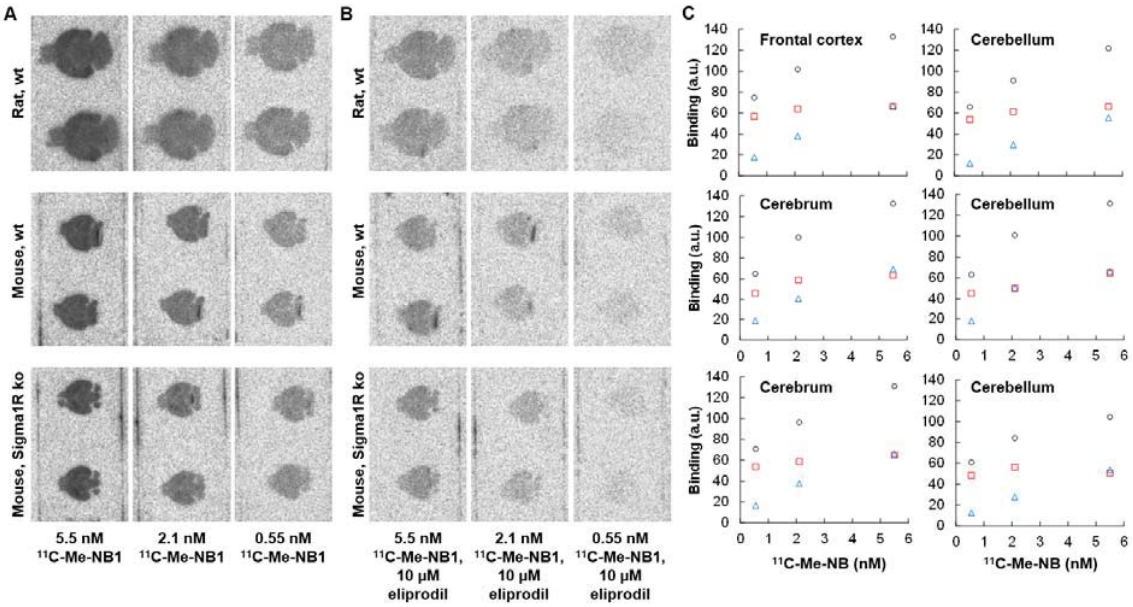

Supplemental Figure 14. *In vitro* autoradiography with brain slices from wt rats, wt mice and Sigma1R ko mice at 5.5 nM, 2.1 nM and 0.55 nM ^{11}C-Me-NB1 as indicated (**A**) and with 10 µM eliprodil for blocking (**B**). **C**) Bound radioactivity was quantified with PMOD v3.8 by region-of-interest analysis for cerebrum (mice), frontal cortex (rat) and cerebellum. The background-corrected radioactivity was averaged for the two brain slices per slide. Black circles, total bound radioactivity (as in **A**, background-corrected). Blue triangles, unspecific binding (as in **B**, background-corrected). Red squares, specifically bound tracer (difference between **A** and **B**). Note that specific binding is saturated already at the lowest investigated ^{11}C-Me-NB1 concentration of 0.55 nM, in agreement with the high affinity observed *in vivo* (**Fig. 2A** and **4A**). Note in addition the high specific binding in cerebellum of wt rat and mouse and of Sigma1R ko mouse, indicating off-target binding but excluding binding to Sigma1R.

Supplemental Tables

Supplemental Table 1 Binding affinities determined with rat brain membranes [a)]

Compound	Tritiated compound	Temperature (°C)	IC_{50} (nM) [b)]	K_i (nM) [c)]	n [d)]
Ro-25-6981	[^{3}H]ifenprodil	20	44.7 ± 11.0 [e)]	42.3 ± 12.0	3
	(+)-[^{3}H]pentazocine	20	23.1	15.4	1
Haloperidol	[^{3}H]ifenprodil	20	~ 8000		1
		37	~ 6000		1
	(+)-[^{3}H]pentazocine	20	753	482	1
		37 [f)]	38.0	31.9	1
Eliprodil	[^{3}H]ifenprodil	20	51.4 ± 33.9, 17-85	48.5 ± 32.0, 16-80	3
	(+)-[^{3}H]pentazocine	37	335-1281	229-875	3
Me-NB1	[^{3}H]ifenprodil	20	42.4 ± 2.9	40.2 ± 2.8	4
	(+)-[^{3}H]pentazocine	37	> 4000		3

[a)] Binding affinities were determined in a competition binding assay with rat brain membranes as described elsewhere (*5*-*7*) with 1 to 5 nM ^{3}H-ifenprodil or (+)-^{3}H-pentazocine (both PerkinElmer, Schwerzenbach, Switzerland). Ifenprodil binds with a K_d of 37 nM to the rat GluN1/GluN2B NTD binding site (*8*)) while (+)-pentazocine binds with a K_d 7 nM to rat Sigma1R (*9*). Sample volumes were 200 µL containing 0.1 mg (for assays with ^{3}H-ifenprodil) or 0.2 mg (assays with (+)-^{3}H-pentazocine) total protein in HEPES buffer (30 mM Na-HEPES, 110 mM NaCl, 5 mM KCl, 2.5 mM $CaCl_2$, 1.2 mM $MgCl_2$ at pH 7.4). Test compounds were added at various concentrations in triplicates and samples were incubated for 1 to 1.5 h at the indicated temperature or 2 to 2.5 h in the case of (+)-^{3}H-pentazocine at 37°C and filtered at 4°C as described elsewhere (*5*). The K_i values were calculated with the Cheng-Prusoff equation from the IC_{50} values determined in the binding assay and K_d of the tritiated compounds for the respective rat receptors, as indicated. [b)] Average ± standard deviation and/or range in case of 3 or more independent experiments, or results of individual experiments; [c)] Calculated with the Cheng-Prusoff equation and ifenprodil K_d =37 nM to rat brain NTD binding site (*8*) and (+)-pentazocine K_d=7 nM to rat Sigma1R (*9*), respectively; [d)] number of independent experiments with triplicates for each test concentration; [e)] similar results at 4°C (n=2) and 37°C (n=2); the mean K_i including all temperatures was 49.8 ± 19.7 nM. [f)] Inverse Sigma1R agonists such as haloperidol induce the formation of Sigma1R tetra- and oligomers, the suggested resting states of Sigma1R (*6*). The reduced form of haloperidol, formed by metabolism, irreversibly inhibits the receptor, in addition (*10*). Both would explain the temperature-dependent competition with (+)-^{3}H-pentazocine. Note that the bivalent cations in the HEPES buffer could affect the binding affinity (*1*).

Supplemental Table 2. Details of the PET scans with input function recording

Scan ID	Treat-ment [a)]	Body weight (g)	Injected dose (MBq)	Injected dose (nmol/kg)
1	V	320.6	31.83	0.44
3	V	352.8	36.47	0.59
5	V	319.1	51.66	0.78
7	V	341.1	33.68	0.47
Average ± SD	V	333.4 ± 16.4	38.41 ± 9.0	0.57 ± 0.15
2	K	328.4	33.16	0.69
4	K	310.7	40.69	0.54
6	K	341.4	38.5	0.46
Average ± SD	K	326.8 ± 15.4	37.5 ± 3.9	0.56 ± 0.12
Average ± SD	V,K	328.9 ± 17.5	39.8 ± 7.4	0.56 ± 0.14

[a)] V, vehicle; K, ketamine (25 mg/kg intraperitoneally, 30 min before tracer).

Supplemental Table 3. Fit composite parameters of the individual scans in Supplemental Table 2.

Scan ID	Treat-ment [a]	Model [b]	$V_{T,fit}$	$V_{T,Logan}$	BP_{ND}	V_S	V_{ND}	SUV (0-60min)	V_T of radio-metabolite	AICc [e]
1	V	2	12.57	12.54	2.67	9.14	3.43	2.94	0.19	266.1
		1	14.44		-	-	-	2.94	0.33	317.9
3	V	2	12.07	12.22	3.46	9.36	2.71	2.58	0.18	236.9
		1	11.87		-	-	-	2.58	0.14	332.7
5	V	2	10.71	10.68	3.19	8.15	2.56	2.41	0.17	250.4
		1	12.36		-	-	-	2.41	0.47	332.7
7 [c]	V	2	-	-	-	-		2.92		
		1			-	-		2.92		
Average ± SD [d]	V	2	11.78 ± 0.96	11.81 ± 0.99	3.11 ± 0.40	8.89 ± 0.64	2.90 ± 0.46	2.72 ± 0.26	0.18 ± 0.01	251.1 ± 14.6
Average ± SD	V	1	12.89 ± 1.37		-	-	-	2.72 ± 0.26	0.31 ± 0.16	327.7 ± 8.5
2 [c]	K	2			-	-	-	2.71		
		1			-	-	-	2.71		
4	K	2	12.34	12.45	5.04	10.30	2.04	2.62	0.05	244.8
		1	16.44		-	-	-	2.62	0.38	341.9
6	K	2	11.49	11.59	4.50	9.40	2.09	2.42	0.15	225.3
		1	14.26		-	-	-	2.42	0.48	379.3
Average ± SD	K	2	11.92	12.02	4.77	9.85	2.07	2.58 ± 0.15	0.10	235.1
Average ± SD	K	1	15.35		-	-	-	2.58 ± 0.15	0.43	360.6
Average ± SD	V,K	2	11.84 ± 0.75	11.90 ± 0.77	3.77 ± 0.97	9.27 ± 0.77	2.57 ± 0.56	2.59 ± 0.21	0.15 ± 0.06	244.7 ± 15.2
Average ± SD	V,K	1	13.87 ± 1.83		-	-	-	2.59 ± 0.21	0.36 ± 0.14	340.9 ± 23.1
Average ± SD	V,K	2 [f]	11.86 ± 0.69	11.75 ± 0.78	3.77 ± 1.01	9.29 ± 0.84	2.57 ± 0.55	2.59 ± 0.21	0	238.8 ± 18.3

[a] V, vehicle; K, ketamine (25 mg/kg intraperitoneally, 30 min before tracer). [b] 1, One-tissue compartment model; 2, two-tissue compartment model for parent tracer. One-tissue compartment model for radiometabolite in both cases. [c] No fit data available (see Methods). [d] SD, standard deviations shown for $n \geq 3$. [e] Corrected Akaike information criterion (Methods); residues are from brain TACs, residues of parent to total radioactivity in brain and plasma were not taken into account. [f] Distribution of the radiometabolite to the brain ignored.

Supplemental Table 4. Fit K_1, k_2, k_3 and k_4 of the individual scans of Supplemental Tables 2 and 3.

Scan ID	Treatment [a]	Model [b]	K_1 (mL/min/cm^3)	k_2 (1/min)	k_3 (1/min)	k_4 (1/min)
1	V	2	2.15	0.63	0.64	0.24
		1	1.70	0.12	-	-
3	V	2	2.42	0.89	0.63	0.18
		1	1.55	0.13	-	-
5	V	2	2.64	1.03	0.75	0.24
		1	1.71	0.14	-	-
7 [c]	V	2	-	-	-	-
		1	-	-	-	-
Average ± SD [d]	V	2	2.40 ± 0.25	0.85 ± 0.21	0.67 ± 0.07	0.22 ± 0.03
Average ± SD	V	1	1.66 ± 0.09	0.13 ± 0.01	-	-
2 [c]	K	2	-	-	-	-
		1	-	-	-	-
4	K	2	2.86	1.40	0.80	0.16
		1	1.64	0.10	-	-
6	K	2	4.38	2.09	0.83	0.19
		1	1.91	0.13	-	-
Average ± SD	K	2	3.62	1.75	0.81	0.17
Average ± SD	K	1	1.77	0.12	-	-
Average ± SD	V,K	2	2.89 ± 0.87	1.21 ± 0.57	0.73 ± 0.09	0.20 ± 0.04
Average ± SD	V,K	1	1.70 ± 0.13	0.12 ± 0.02	-	-
Average ± SD	V,K	2 [e]	2.91 ± 0.87	1.21 ± 0.56	0.74 ± 0.09	0.20 ± 0.04

[a] V, vehicle; K, ketamine (25 mg/kg intraperitoneally, 30 min before tracer). [b] 1, One-tissue compartment model; 2, two-tissue compartment model for parent tracer. One-tissue compartment model for radiometabolite in both cases. [c] No fit data available (see Methods). [d] SD, standard deviations shown for $n \geq 3$. [e] Distribution of the radiometabolite to the brain ignored.

References Supplemental Information

1. Mutel V, Buchy D, Klingelschmidt A, et al. In vitro binding properties in rat brain of [3H]Ro 25-6981, a potent and selective antagonist of NMDA receptors containing NR2B subunits. *J Neurochem.* 1998;70:2147-2155.

2. Krämer SD. Positron Emission Tomography (PET): Quantification and Kinetic Modeling. *Reference Module in Chemistry, Molecular Sciences and Chemical Engineering*. Amsterdam (NL): Elsevier; 2015.

3. Logan J, Fowler JS, Volkow ND, et al. Graphical analysis of reversible radioligand binding from time-activity measurements applied to [N-11C-methyl]-(-)-cocaine PET studies in human subjects. *J Cereb Blood Flow Metab.* 1990;10:740-747.

4. Cunningham VJ, Rabiner EA, Slifstein M, Laruelle M, Gunn RN. Measuring drug occupancy in the absence of a reference region: the Lassen plot re-visited. *J Cereb Blood Flow Metab.* 2010;30:46-50.

5. Milicevic Sephton S, Mu L, Schweizer WB, Schibli R, Krämer SD, Ametamey SM. Synthesis and evaluation of novel alpha-fluorinated (E)-3-((6-methylpyridin-2-yl)ethynyl)cyclohex-2-enone-O-methyl oxime (ABP688) derivatives as metabotropic glutamate receptor subtype 5 PET radiotracers. *J Med Chem.* 2012;55:7154-7162.

6. Chu UB, Ruoho AE. Sigma receptor binding assays. *Curr Protoc Pharmacol.* 2015;71:1 34 31-21.

7. Nguyen VH, Kassiou M, Johnston GA, Christie MJ. Comparison of binding parameters of sigma 1 and sigma 2 binding sites in rat and guinea pig brain membranes: novel subtype-selective trishomocubanes. *Eur J Pharmacol.* 1996;311:233-240.

8. Schoemaker H, Allen J, Langer SZ. Binding of [3H]ifenprodil, a novel NMDA antagonist, to a polyamine-sensitive site in the rat cerebral cortex. *Eur J Pharmacol.* 1990;176:249-250.

9. Cagnotto A, Bastone A, Mennini T. [3H](+)-pentazocine binding to rat brain sigma 1 receptors. *Eur J Pharmacol.* 1994;266:131-138.

10. Cobos EJ, del Pozo E, Baeyens JM. Irreversible blockade of sigma-1 receptors by haloperidol and its metabolites in guinea pig brain and SH-SY5Y human neuroblastoma cells. *J Neurochem.* 2007;102:812-825.